SUPPLEMENTARY INFORMATION

Raphaël Maire, Andrea Plati, Frank Smallenburg and Giuseppe Foffi

A Details on numerical simulations

A.1 Forces, Potential and Box

Using LAMMPS, we simulate a deformable, periodic, two-dimensional box of constant height and width L. The box undergoes simple shear characterised by a shear strain γ along the x direction, resulting in a tilted simulation cell with lattice vectors:

$$\boldsymbol{a}_x = (L,0), \quad \boldsymbol{a}_y = (\gamma L, L). \tag{S1}$$

N particles of mass m are placed in the box, which defines the density: $\rho = N/L^2$. Particles interact through a smoothed force of the form:

$$F_{\text{smoothed}}(r) = \left(-\frac{\mathrm{d}U}{\mathrm{d}r}\right) S_{\text{mollifier}}(r; r_{\text{thres}}, r_{\text{cut}}), \qquad \frac{U(r)}{\varepsilon} = \left[\left(\frac{\sigma}{r}\right)^{14} + \frac{1}{2}\left(1 - \tanh\left(\frac{r-\delta}{w}\right)\right)\right] \tag{S2}$$

where $S_{\text{mollifier}}(r; r_{\text{thres}}, r_{\text{cut}})$ is a mollifier defined as:

$$S(r; r_{\text{thres}}, r_{\text{cut}}) = \begin{cases} 1, & r \le r_{\text{thres}}, \\ \exp\left[1 - \dfrac{1}{1 - \left(\frac{r - r_{\text{thres}}}{r_{\text{cut}} - r_{\text{thres}}}\right)^2}\right], & r_{\text{thres}} \le r \le r_{\text{cut}}, \\ 0, & r \ge r_{\text{cut}}. \end{cases} \tag{S3}$$

This smoothing procedure ensures that both the force F_{smoothed} and the potential $U_{\text{smoothed}}(r) \equiv \int_r^{r_{\text{cut}}} F_{\text{smoothed}}(r')\mathrm{d}r'$ vanish smoothly to 0 at the cut-off r_{cut}, starting from r_{thres}. Throughout our simulations, we chose $w = 0.1\sigma$, $\delta = 1.35\sigma$, $r_{\text{thres}} = 1.85\sigma$ and $r_{\text{cut}} = 1.95\sigma$. The original and smoothed potentials and forces are shown in Fig. S1. To facilitate efficient computation in LAMMPS, we tabulate the force and potential on 2000 evenly spaced points between $r = 0.6\sigma$ to $r = r_{\text{cut}} = 1.95\sigma$. During the simulation, the values are obtained via spline interpolation using the `pair_style table spline 2000` command. The sampling is illustrated in the inset of Fig. S1.

The stresses are measured in LAMMPS via the virial stress.

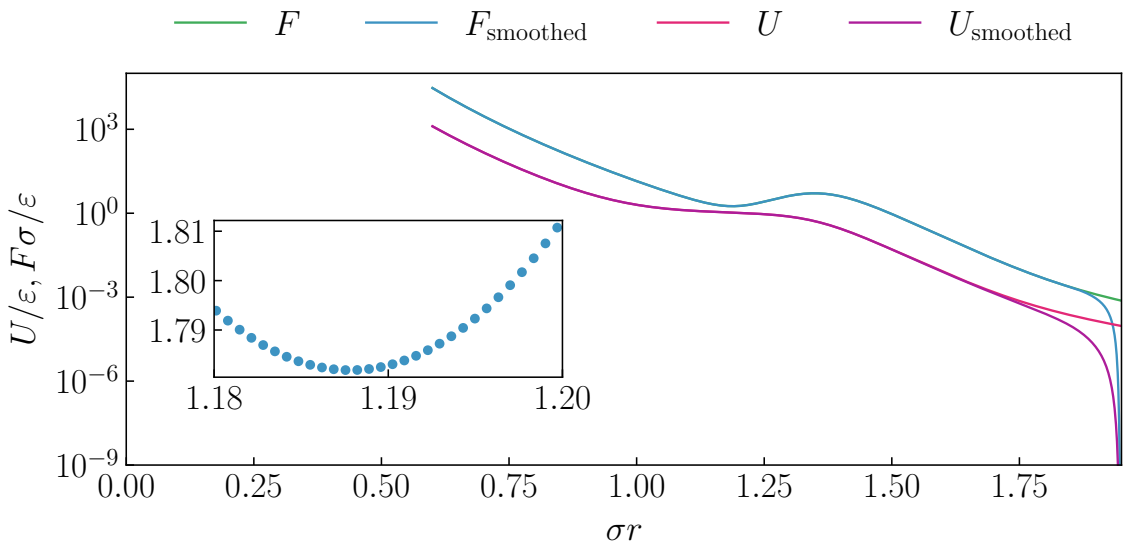

Fig. S1 Smoothed forces and potential. In the inset, we show the typical sampling of points used for the tabulated force.

A.2 Equilibrium thermalisation

For simulations requiring an initial thermalised configuration, we equilibrate the system at a target temperature T using a Langevin thermostat with LAMMPS damping coefficient $0.1\sqrt{m\sigma^2/\varepsilon}$ and timestep $0.001\sqrt{m\sigma^2/\varepsilon}$. The system is annealed from an initial temperature $k_BT/\varepsilon = 1$, which is linearly decreased to the desired value T. The annealing is performed over 10^7 timesteps for systems with

$N \leq 2 \times 10^4$, and 10^8 timesteps for larger systems. The system is then held at the target temperature for an additional 10^7 timesteps. We verified that both the potential energy and the pressure reach statistically stationary values following this procedure.

A.3 Athermal quasi-static shear (AQS)

Starting from a given configuration in an undeformed square box, we perform athermal quasi-static shear (AQS). Each AQS step consists of an affine shear increment $\gamma \to \gamma + \Delta\gamma$ with $\Delta\gamma = 10^{-4}$ followed by energy minimisation via Conjugate Gradient descent with a force tolerance of $10^{-10}\varepsilon/\sigma$. This two-step procedure is repeated until the box strain reaches $\gamma_{\max}$. For cyclic shear, once $\gamma_{\max}$ is reached, we reverse the sign of $\Delta\gamma$ and continue the simulation.

If $\gamma_{\max}/\Delta\gamma$ is not an integer, the deformation may slightly exceed $\gamma_{\max}$; in such cases, we reset the strain to exactly $\gamma \to \gamma_{\max}$ and re-minimise the energy. Similarly, when the strain changes from negative to positive values, we reset the strain to $\gamma \to 0$ to ensure that the system is analysed in an exactly undeformed box.

A.4 Finite shear rate

For simulations involving a finite shear rate, we perform overdamped dynamics using the `Brownian` fix of `LAMMPS` at zero temperature:

$$\frac{d\gamma}{dt} = \dot{\gamma} \qquad \Gamma \frac{d\mathbf{r}_i}{dt} = -\frac{\partial U}{\partial \mathbf{r}_i}, \tag{S4}$$

where $\dot{\gamma}$ is the imposed strain rate. The box deformation thus evolves according to $\gamma(t) = \dot{\gamma} t$ (in between strain-rate reversal events), and the particle equations of motion are integrated simultaneously with the box shear. The timestep is set to $0.001\Gamma\sigma^2/\varepsilon$.

B Ground state phase diagram

B.1 Energy of each phase

The $T = 0$ phase diagram can be obtained straightforwardly since the free energy density $f = (E - TS)/L^2$ reduces simply to the ground-state energy density. We compare the energies of the square and hexagonal lattices in Fig. S2 and determine the coexistence densities using a Maxwell construction. In the same figure, we also verify that a random Stampfli tiling [122], or a random "mean-field" tiling (as described below) with a fraction x_S of squares and $1 - x_S$ of triangles, always has a higher energy than the square-hexagonal coexistence. Therefore, such tilings do not represent the stable phase, contrary to the claim made in Ref. 96. While this does not exclude the possibility that a more complex quasicrystalline structure could be stable at $T = 0$, it provides strong evidence that, at equilibrium, the quasicrystal is instead stabilised by entropy.

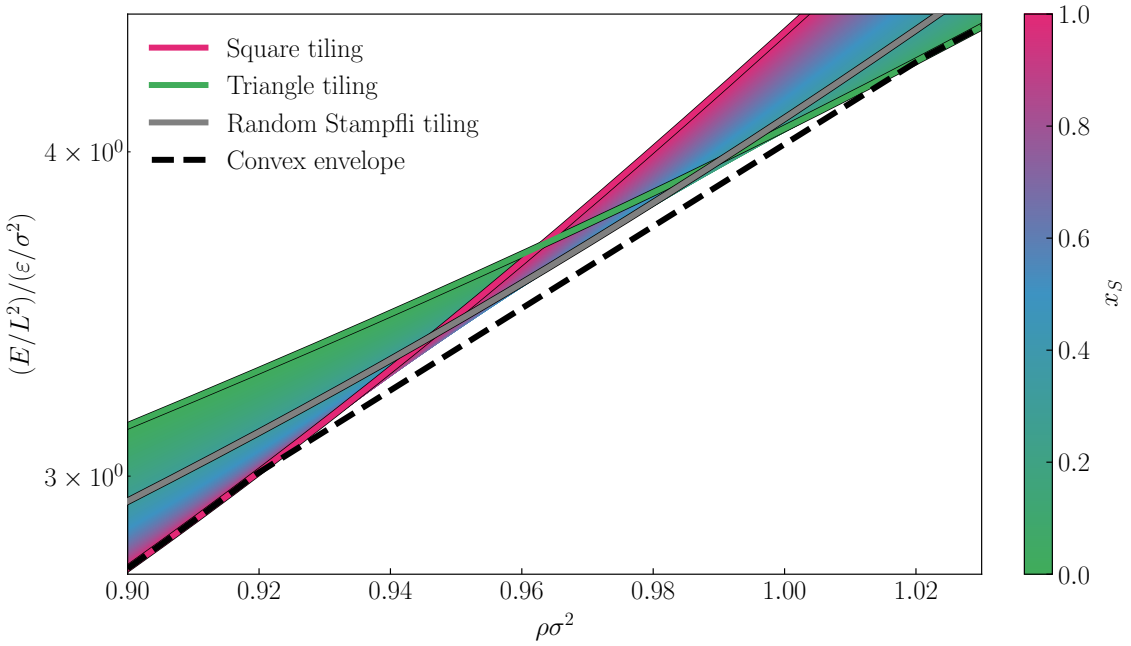

Fig. S2 Energy of the square, triangle, Stampfli, and random "mean-field" (in shade of colour) tiling as a function of the density. The lowest energy state is never a random tiling. The y-axis is logarithmically scaled for better visualisation.

We now clarify what we mean by a "random mean-field" tiling.

B.2 Random "mean-field" tiling

We compute the typical energy of a random tiling in the mean-field limit. By mean-field, we mean that each particle is assumed to experience an average (possibly non-integer) number of neighbours, that the positions of triangles and squares are uncorrelated, and that each nearest neighbour bond is the same length s. This excludes coexistence, where triangle and square regions would have different bond lengths.

Let f_T, f_S, and $f = f_S + f_T$ denote the number of triangles, squares, and total tiles per unit of area, respectively. The fraction of square and triangle tiles is given by:

$$x_S = \frac{f_S}{f_T + f_S} \quad \text{and} \quad x_T = 1 - x_S. \tag{S5}$$

The areas of square and triangle tiles are obtained from their edge length s:

$$A_S = s^2 \quad \text{and} \quad A_T = \frac{\sqrt{3}}{4} s^2. \tag{S6}$$

Since we perfectly tile the plane, we must have:

$$f_T A_T + f_S A_S = 1 \Rightarrow (1 - x_S) f \frac{\sqrt{3}}{4} s^2 + x_S f s^2 = 1, \tag{S7}$$

where f and s are the unknown.

Determination of f: The number of edges per unit area e is given by:

$$e = \frac{3 f_T + 4 f_S}{2} = \frac{3 + x_S}{2} f \tag{S8}$$

where the factor 2 comes from the fact that each edge is shared by two tiles. We now use Euler's identity, using the fact that the number of vertices is equal to the particle density:

$$\rho - e + f = 0 \Rightarrow f = \frac{2\rho}{1 + x_S} \tag{S9}$$

Determination of s: Replacing Eq. (S9) into Eq. (S7) leads to an expression for the edge length:

$$s = \sqrt{\frac{1 + x_S}{2\rho \left(x_S + (1 - x_S) \frac{\sqrt{3}}{4} \right)}}, \tag{S10}$$

which interpolates smoothly between the known result $\rho s^2 = \frac{2}{\sqrt{3}}$ for the hexagonal lattice ($x_S = 0$) and $\rho s^2 = 1$ for the square lattice ($x_S = 1$).

Determination of the number of closest neighbours: To obtain the energy of the system at the *mean-field level*, we must find the *average* number of closest neighbours z per vertex, which are at distance s. Since each edge connects two vertices, we find:

$$z = \frac{2e}{\rho} = \frac{2(3 + x_S)}{1 + x_S}, \tag{S11}$$

which interpolates smoothly between $z = 4$ for a square lattice and $z = 6$ for a hexagonal lattice.

Determination of the number of second-closest neighbours: Since the energy cut-off is at 1.95σ, we need to consider second-nearest neighbours. We will neglect the one arising from the triangles that lie at a distance $\sqrt{3}s$ (which should be negligible for densities below $\rho\sigma^2 \simeq 1$ since $U(1.75\sigma) \simeq 10^{-3}\varepsilon$) and only consider the ones arising from squares, lying at $\sqrt{2}s$. Since each square has two diagonals with two particles each, the number of second-closest neighbours z_2 per vertex is:

$$z_2 = 4 \frac{f_S}{\rho} = \frac{8 x_S}{1 + x_S}, \tag{S12}$$

which vanishes in the absence of squares and reaches 4 for a perfect square lattice.

Determination of the potential energy: The potential energy is:

$$E = \frac{1}{2} z U(s) + \frac{1}{2} z_2 U(\sqrt{2}s). \tag{S13}$$

We neglected contributions beyond second-nearest neighbours and assumed that each particle experiences, on average, z neighbours and z_2 second-closest neighbours (note that z and z_2 do not have to be integers).

C Self-assembly speed

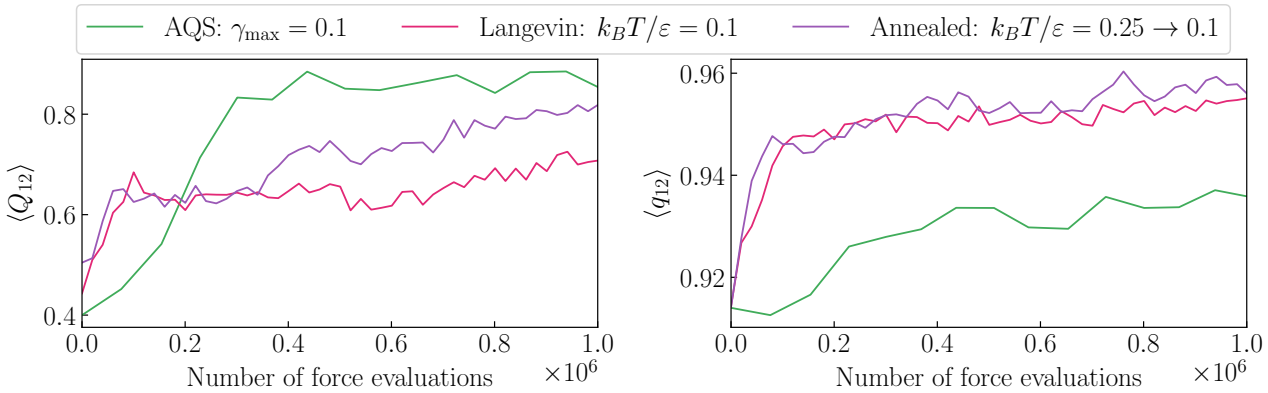

Fig. S3 Self-assembly speed, measured via the local and global 12-fold bond-orientational parameters, in terms of the number of force evaluations. All systems are taken at $\rho\sigma^2 = 0.95$ and $N = 3000$. "AQS" is a system simulated via the quasistatic sheared protocol described in the main text at $\gamma_{\max} = 0.1$, "Langevin" is a system self-assembled via a Langevin bath at equilibrium and temperature $k_BT/\varepsilon = 0.1$ and "Annealed" is a system self-assembled by decreasing linearly the temperature with time, from $k_BT/\varepsilon = 0.25$ to 0.1.

In Fig. S3, we report the typical self-assembly time, measured in terms of the number of force evaluations, for three cases: an AQS protocol, a system thermalized with a Langevin bath, and a thermally annealed system. We find that the AQS protocol typically leads to faster quasicrystal self-assembly than the thermal protocol, for the chosen target temperature.

D System size scaling of $\langle Q_{12} \rangle$

To obtain the scaling of $\langle Q_{12} \rangle$ with system size, it is easier to deal with:

$$\langle Q_{12}^2 \rangle \equiv \left\langle \frac{1}{N^2} \sum_{j \neq k} q_{12}^{(j)} q_{12}^{*(k)} \right\rangle. \tag{S14}$$

$\langle Q_{12} \rangle$ should behave roughly as $\sqrt{\langle Q_{12}^2 \rangle}$. We define the correlation function:

$$C_{12}(r) = \frac{\left\langle \sum_{j \neq k} q_{12}^{(j)} q_{12}^{*(k)} \delta(r - |\mathbf{r}_j - \mathbf{r}_k|) \right\rangle}{\left\langle \sum_{j \neq k} \delta(r - |\mathbf{r}_j - \mathbf{r}_k|) \right\rangle}. \tag{S15}$$

To obtain the continuum form, we perform some manipulation on the following:

$$\begin{aligned} \langle Q_{12}^2 \rangle = \frac{1}{N^2} \left\langle \sum_{j \neq k} q_{12}^{(j)} q_{12}^{*(k)} \right\rangle &= \left\langle \sum_{j \neq k} \int_0^L q_{12}^{(j)} q_{12}^{*(k)} \delta(r - r_{jk}) dr \right\rangle \\ &= \int \left\langle \sum_{j \neq k} q_{12}^{(j)} q_{12}^{*(k)} \delta(r - r_{jk}) \right\rangle dr \\ &= \int C_{12}(r) \left\langle \sum_{j \neq k} \delta(r - r_{jk}) \right\rangle dr \\ &= \frac{\rho}{N} \int_{[0,L_x] \times [0,L_y]} C_{12}(r) g(r) d^2\mathbf{r}. \end{aligned} \tag{S16}$$

Where we recognised the pair-correlation function $g(r)$. At large distances, $g(r) \simeq 1$, therefore, we obtain, for large L, the scaling of $\langle Q_{12} \rangle$:

$$\langle Q_{12} \rangle \sim \sqrt{\frac{1}{N} \int_0^L r C_{12}(r) dr} \sim \begin{cases} N^0 & \text{if} \quad C_{12}(r \to \infty) = c_0 \\ N^{-\eta/4} & \text{if} \quad C_{12}(r \to \infty) \sim r^{-\eta} \text{ with } 0 < \eta < 2 \\ N^{-1/2} & \text{if} \quad C_{12}(r \to \infty) \sim e^{-r/\xi} \text{ or } C_{12}(r \to \infty) \sim r^{-\eta'} \text{ with } \eta' > 2 \end{cases} \tag{S17}$$

The N^0 scaling corresponds to a system with a well-defined orientation in the infinite system size limit. In this case, it is orientationally long-range ordered. The $N^{-\eta/4}$ scaling describes a slow decrease of global orientation with system size. The orientational order is only quasi-long ranged. In the last case, the orientational order is lost as $N^{-1/2}$, which is the central limit theorem; we say that the orientational order is short-ranged (note that this scaling can also be obtained with a strong power-law decay of the correlation function).